Statistical Distributions of Plasma Density and Pressure in the Jovian Plasma Sheet

Haobo Fu, Chao Yue, Qianli Ma, M. Blanc, Q. -G. Zong, Xuzhi Zhou, B. H. Mauk, Zhiyang Liu

The Astrophysical Journal, 972:22 (13pp), 2024 September 1 https://doi.org/10.3847/1538-4357/ad58dd

Statistical Distributions of Plasma Density and Pressure in the Jovian Plasma Sheet

Haobo Fu[1], Chao Yue[1], Qianli Ma[2,3], M. Blanc[4], Q.-G. Zong[1], Xuzhi Zhou[1], B. H. Mauk[5], and Zhiyang Liu[1,4]
[1] Institute of Space Physics and Applied Technology, Peking University, Beijing, People's Republic of China
[2] Department of Atmospheric and Oceanic Sciences, University of California, Los Angeles, CA, USA
[3] Center for Space Physics, Boston University, Boston, MA, USA
[4] Institut de Recherche en Astrophysique et Planetologie (IRAP), CNRS-Universite Toulouse III Paul Sabatier-CNES, Toulouse, France
[5] The Johns Hopkins University Applied Physics Laboratory, Laurel, MD, USA
Received 2023 November 2; revised 2024 June 2; accepted 2024 June 10; published 2024 August 22

Abstract

The Jovian plasma sheet is a key region of the Jovian magnetosphere populated by a mix of warm and hot plasma. It is the main channel for radial transport of mass and energy in the Jovian magnetosphere and provides a favorable environment for magnetic reconnection and wave–particle interactions although the understanding of its plasma properties is incomplete. This study combines observations from the Jovian Auroral Distributions Experiment and Juno Energetic Particle Detector Instrument on board the Juno spacecraft during its first 31 orbits to analyze the plasma properties of the Jovian plasma sheet from 20 R_J to 100 R_J. Our results indicate that the plasma number density decreases from 1 cm^{-3} at 20 R_J to 0.005 cm^{-3} at 100 R_J, while the plasma pressure decreases from 2 nPa at 20 R_J to 0.02 nPa at 100 R_J. The plasma pressure inside the plasma sheet is comparable to the magnetic pressure in the lobe region, suggesting a rough balance between the two. In the plasma sheet with $r > 70\,R_J$, the H^+ density and pressure remain relatively constant, likely due to other plasma sources such as the solar wind. Additionally, we find that the pressure (density) ratios for heavy ions between the center and the edge of the plasma sheet are generally an order of magnitude, while that for H^+ decreases with radial distance. These findings contribute to a more comprehensive understanding of the plasma properties of the Jovian plasma sheet.

Unified Astronomy Thesaurus concepts: Planetary magnetospheres (997); Planetary science (1255); Planetary-disk interactions (2204)

1. Introduction

Jupiter possesses the largest planetary magnetosphere in the solar system, with its magnetopause located between 60 and 100 R_J ($1R_J = 71{,}492$ km). Io, the closest to Jupiter among the Galilean moons, orbiting at approximately 5.9 R_J from Jupiter, continuously releases dust and neutral gas rich in oxygen and sulfur through volcanic activity, forming a neutral cloud that is ionized by electron impact and charge exchange and creates a plasma torus along its orbit (as reviewed by Thomas et al. 2004; Bagenal & Dols 2020). Due to the centrifugal force, the torus plasma is transported outward by a variety of processes, including the interchange instability (see reviews by Khurana et al. 2004; Thomas et al. 2004), forming a thin plasma sheet several Jupiter radii thick, also sometimes referred to as the current sheet or the magnetodisk (Vasyliunas 1983). This plasma sheet rigidly corotates with Jupiter in an approximately 10 hr period within approximately 20 R_J. Its lag to corotation then progressively increases at larger radial distances under the coupled effects of outward angular momentum transport and the electrodynamical coupling of the Jovian upper atmosphere, as described initially by Hill (1979) and later by Cowley & Bunce (2001) and Cowley et al. (2003). Observations from the Voyager and Galileo spacecraft revealed the plasma properties of the Jovian plasma sheet at distances of 5–50 R_J (e.g., Khurana et al. 2004; Krupp et al. 2004; Mauk et al. 2004; Bagenal et al. 2016, 2017b; Bodisch et al. 2017; Dougherty et al. 2017), leading to the development of radial distribution models of various plasma parameters in the plasma sheet (Bagenal & Delamere 2011; Nichols et al. 2015).

In recent years, NASA's Juno mission has provided a wealth of new observational data for the study of Jupiter. Due to its highly eccentric orbit, Juno provides in situ observations ranging from the magnetosheath plasma beyond 100 R_J to the precipitating particles within 2 R_J (e.g., Ranquist et al. 2019; Bandyopadhyay et al. 2022; Mauk et al. 2022). The long-term magnetic field data collected by Juno over the years have laid a solid foundation for statistical analysis and modeling of the Jovian magnetosphere and plasma sheet (e.g., Connerney et al. 2018, 2020; Liu et al. 2021). Additionally, the particle detectors carried on board Juno have provided new observations of charged particles in the Jovian magnetosphere and plasma sheet (e.g., Allegrini et al. 2020, 2021; Wang et al. 2021; Szalay et al. 2022). For instance, Kim et al. (2020a, 2020b) and Wang et al. (2024) used Jovian Auroral Distributions Experiment (JADE) data to calculate the ion composition and temperature distribution from 10 R_J to ~50 R_J, differentiating oxygen and sulfur ions. Huscher et al. (2021) also utilized these data to statistically analyze the number density distribution of different components within 50 R_J. Furthermore, Ma et al. (2021) presented the radial distributions of the electron flux, phase-space density (PSD), and pitch-angle distributions in the energy range from 0.1 to 1000 keV.

However, direct observations of Jovian plasma parameters are primarily concentrated within 50 R_J, and few studies have simultaneously considered observations from JADE and Juno Energetic Particle Detector Instrument (JEDI). Additionally, our understanding of the latitudinal variations of the Jovian plasma sheet remains limited. In this study, we utilize observations from both JADE and JEDI on board Juno during

its first 31 orbits to statistically analyze plasma properties in the plasma sheet within the 20–100 R_J range and investigate their radial and latitudinal variations. Our findings contribute to a more comprehensive understanding of the plasma properties in the Jovian plasma sheet.

2. Data and Method

2.1. Juno Data

The Juno spacecraft, launched in 2011 August, entered Jovian orbit in 2016 July. The perijove of Juno's highly eccentric orbit is approximately 1.05 R_J, and its apojove is around 110 R_J. The spin-stabilized spacecraft rotates around the axis of its high-gain antenna with a spin period of 30 s.

To study the plasma parameters of the Jovian plasma sheet, we use data from several Juno instruments. The fluxgate magnetometer (MAG; Connerney et al. 2017) provides measurements of the three-component magnetic field with a time resolution of up to 64 Hz, allowing us to determine the relative position of the plasma sheet. We use the recently released L5 electron and ion time-of-flight (TOF) data from JADE (McComas et al. 2017) and calibrated data from JEDI (Mauk et al. 2017) to analyze the plasma parameters. We took the *data sigma* provided by the L5 JADE data as the standard deviation. We calculated the Poisson statistics from the counts provided by the JEDI instrument. The standard deviations of the exported quantities are calculated based on error propagation.

JADE consists of an ion detector (JADE-I) and three identical electron detectors (JADE-E). JADE-I is a top-hat electrostatic analyzer with a TOF spectrometer, providing ion observations in the energy range of 10 eV e^{-1} to 46.2 keV e^{-1}. JEDI comprises three sensors with solid-state detectors and microchannel plates, measuring the energy and pitch-angle distributions of energetic electrons, protons, and heavy ions.

Based on the energy-per-charge (E/q)-TOF relation suggested by Kim et al. (2020a), as shown in Figure A1, we assumed ions measured by JADE-TOF with $M/q < 1.3$ amu e^{-1} to be protons and considered heavy ions with 5 amu $e^{-1} < M/q < 21$ amu e^{-1}, which are mainly composed of oxygen and sulfur. In addition, we have excluded ion measurements with uncertainties over 10 times the signal based on the standards from Huscher et al. (2021). We also excluded ion data from JEDI "TOF × pulse height (PH)," and because of proton contamination of the heavy ions and the noncalibration of the lowest energy TOF × PH proton channel (e.g., Mauk et al. 2023), only data from JEDI "TOF × energy (E)" are used. We adopted the assumption used by Huscher et al. (2021) that O^+ and S^{2+} have the same number density with a charge quantity of 1.5e and a mass of 24 amu, forming the basis for calculating the plasma parameters in the plasma sheet.

2.2. Plasma Sheet Crossings and Lobe Regions

We relied on magnetic field observations from the MAG instrument to determine the spacecraft position relative to the plasma sheet. Figure 1(a) illustrates these observations on 2018 October 27 in a spherical coordinate based on the Jupiter–Sun–orbit (JSO) coordinate system defined by Bagenal et al. (2017a). Reversals of the B_r component indicate spacecraft crossings through the plasma sheet. Following Liu et al. (2021), we identified Juno crossings through the Jupiter plasma sheet based on the following conditions:

1. Reversal of the magnetic field B_r component.
2. Radial distance in the R–Phi plane between 20 and 100 R_J.
3. At least a 10 minute period of stable B_r component ($\sigma < 0.1\bar{B}$) within 1 hr before and after the reversal.
4. The averages of B_r in the 1 hr intervals before and after the reversal are opposite.
5. JADE provides observational results with a time resolution smaller than 300 s during the plasma sheet crossing.

Applying the criteria mentioned above, we identified 419 plasma sheet crossing events, as shown in Figure 1(b).

Additionally, we selected lobe regions outside the plasma sheet for comparison using the following criteria:

1. Radial distance in the R–Phi plane between 20 and 100 R_J.
2. Juno's latitude is between ±10°, and its distance to the R–Phi plane is within 10 R_J.
3. Contribution of the magnetic field in the B_r and B_{phi} directions to the total magnetic pressure larger than 99%.
4. Magnetic field stability ($\sigma > 0.1\bar{B}$) for at least 3 hr.

We identified 468 lobe region crossings using this criteria, as illustrated in Figure 1(c).

2.3. Calculations of Plasma Properties

Figure 2 shows an example of the distributions of flux and PSD of electrons, protons, and heavy ions 10 minutes before and after the current-sheet crossing at 05:43 on 2018 October 27 (the gray area shown in Figure 1(a)) at 38.9R_J. More examples of plasma sheet crossings at different radial distances 66.8, 75.2, 86.1, and 96.3 R_J can be found in Figures B1–B4 of Appendix A. We used Level 5 data from JADE for electrons with energy ranging from 0.1 to 100 keV and the JADE-TOF data for protons and heavy ions with energy ranging from 15 eV e^{-1} to 46 keV e^{-1}. The energy of electrons, protons, and heavy ions from JEDI data ranges from ∼100 keV up to ∼MeV. To avoid possible inconsistencies between JADE and JEDI measurements, we excluded JEDI data with fluxes higher than that of the highest energy channel of JADE and expanded the energy range corresponding to channels on both sides of the energy gap to get the full energy coverage. Using the particle observations from JADE and JEDI, we calculated the number density (n) and pressure (P) of each plasma component using the equation:

$$n = 4\pi \int \sqrt{\frac{m}{2E}}\, J(E)\, dE$$

$$P = \pi\sqrt{2m} \int J(E)\sqrt{E}\, dE,$$

where J is the measured ion flux, m represents the particle mass, and E is the particle energy.

To correct the contribution of the bulk velocity v_b to the calculation of plasma thermal pressure of the heavy ions, we assumed the heavy ions have a shifted distribution with a bulk velocity v_b and subtracted its contribution to the energy density based on Koenig's theorem. The thermal pressure (P) is

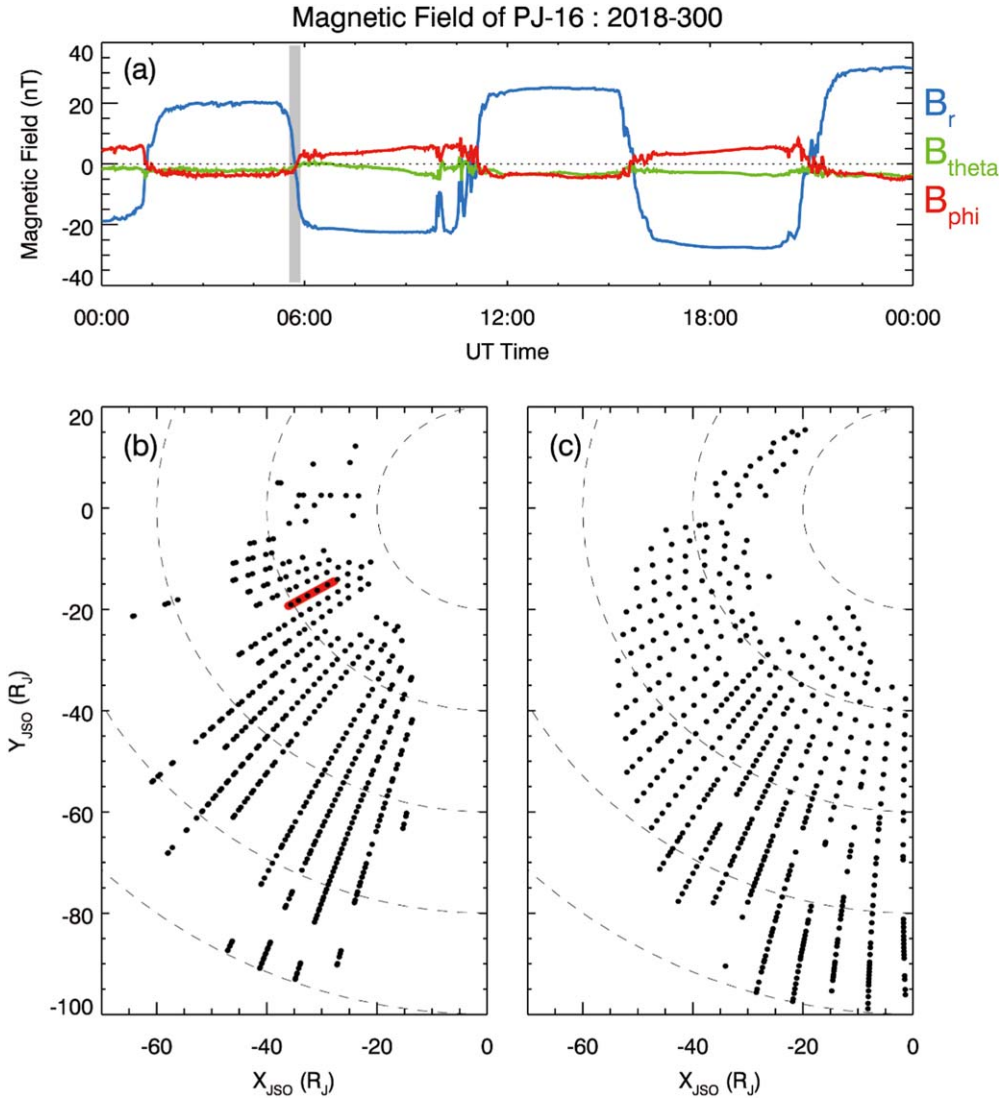

Figure 1. Juno observations of the magnetic field and the distributions of the current-sheet crossings and the lobe regions. Panel (a) shows the three-component magnetic field in JSO spherical coordinates on 2018 October 27. Panels (b)–(c) represent the distribution of current-sheet crossings and lobe regions obtained in Section 2.2. Red region in panel (b) represent the trajectory during 2018 October 27.

calculated using the equation:

$$P_{\text{heavy}} = \pi\sqrt{2m}\int J(E)\sqrt{E}\,dE - \frac{nmv_b^2}{3},$$

where v_b represents the bulk velocity of the plasma, approximated by the peak of heavy ions' PSD as illustrated in Figure 2(f), this peak in heavy ion spectra is well formed and easy to identify, indicating that our estimate of v_b is reliable. If no PSD peak is identified, which indicates that the thermal distribution of the heavy ions submerges the bulk velocity, we choose a lower bound of v_b ($\sim$150 km s^{-1}) to substitute into the formula and calculate the pressure.

3. Results

3.1. Analysis of a Typical Plasma Sheet Crossing Event

Figure 3 illustrates a plasma sheet crossing event between 04:40 and 06:40 UT on 2018 October 27. The magnetic field component B_r (blue line in Figure 3(a)) experienced a reversal at $\sim$05:43 UT, indicating the plasma sheet crossing. Simultaneously, there were significant increases in the fluxes of electrons, protons of several keV, and heavy ions of tens of keV. The proton density (black line in Figure 3(e)) slightly increased as the spacecraft entered the center of the plasma sheet, while the density of heavy ions (red line in Figure 3(e)) notably increased from $\sim$0.01 to $\sim$0.07 cm^{-3}. In the center of the plasma sheet, the magnetic pressure (blue line in Figure 3(f)) decreased, while the pressures of ions and electrons (red and green lines in Figure 3(f)) increased significantly. The total pressure (black line in Figure 3(f)) shows no significant changes, indicating a general balance between the thermal pressure of the plasma in the center of the plasma sheet and the magnetic pressure in the lobe regions.

During this plasma sheet crossing event, the density of heavy ions was significantly larger than that of protons in the center of the plasma sheet. However, at the outer edge of the plasma sheet, the number density of heavy ions decreased significantly and became similar to that of protons, suggesting a tendency for heavy ions to concentrate in the center of the plasma sheet, while hydrogen ions distributions were more dispersed. This

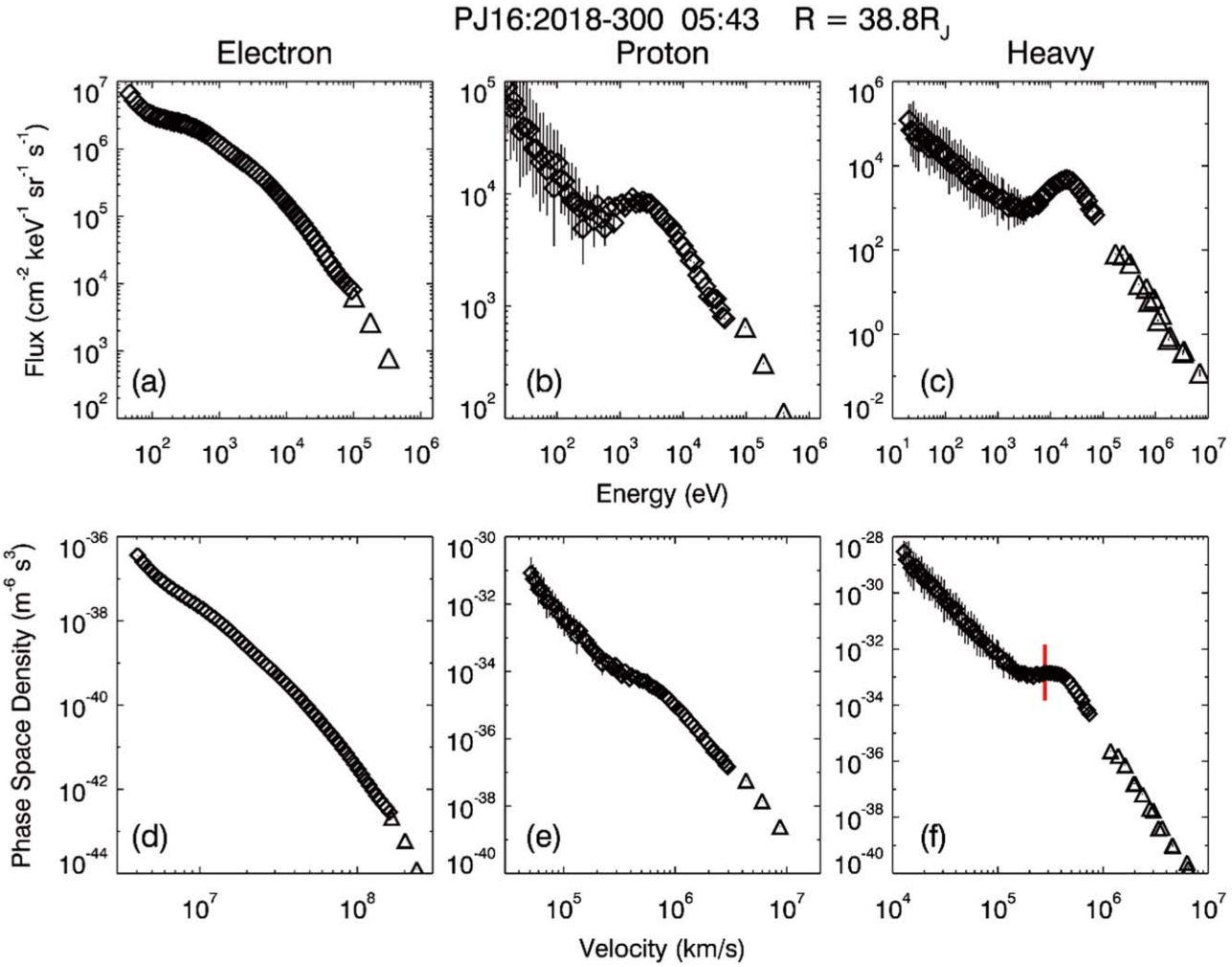

Figure 2. Distributions of flux and PSD of electrons, protons, and heavy ions in the gray area of Figure 1(a). Panels (a)–(c) represent the fluxes, and panels (d)–(f) represent the phase-space densities of each particle species, respectively. The diamonds represent data points from the JADE instrument, and triangles represent the "TOF × E" data from the JEDI instrument, respectively. The red vertical line at ∼300 km s^{-1} in panel (f) represents the PSD local maximum and the approximated bulk velocity. The size of the symbols has no specific meaning.

feature is consistent with diffusive equilibrium theory along the magnetic field or ambipolar diffusion (e.g., Bagenal 1994; Dougherty et al. 2017).

3.2. Radial Distribution of Plasma Properties

To analyze the radial distribution of plasma properties within the Jovian plasma sheet, we selected their average values over 10 minutes before and after the B_r reversal as representative of the plasma properties at the center of the plasma sheet. Figure 4 shows the resulting radial distributions of the number density of electrons, H^+ ions, and heavy ions in the plasma sheet (Figures 4(a)–(c)) and compares different plasma components (Figure 4(d)). The electron density decreases from ∼0.5 cm^{-3} near 20 R_J to around 0.003 cm^{-3} near 100 R_J. Similar to electrons, the densities of proton and heavy ions gradually decrease as the radial distance increases, and heavy ions exhibit larger variations at any specific radial position (Figures 4(b) and (c)). The densities of electrons and heavy ions are generally larger than that of H^+ ions as shown in Figure 4(d).

Figure 5 displays the radial profile of plasma pressure at the center of the plasma sheet. Figures 5(a)–(c) show the pressure distributions of electrons, H^+ ions, and heavy ions, while Figure 5(d) compares the total plasma pressure at the plasma sheet and the magnetic pressure in the lobe regions. The total plasma pressure at the center of the plasma sheet decreases from ∼2 nPa near 20 R_J to ∼0.03 nPa near 100 R_J. Among the plasma components, heavy ions contribute the most to the plasma pressure, while electrons contribute the least. Compared to heavy ions and electrons, the pressure distribution of protons is more dispersed, which may be due to the larger variation of proton flux at any specific location. The plasma pressure is comparable in magnitude with the magnetic pressure in the lobe regions although the plasma sheet pressure seems larger than the magnetic pressure in the lobe regions at similar radial distances ($R_{R\text{-}Phi}$), which may be related to the partial contribution of plasma pressure in the lobe region and the uncertainties of the plasma measurement. The result indicates that the magnetic pressure in the lobe regions primarily balances the thermal pressure in the center plasma sheet.

Additionally, for $r > 70\,R_J$, the proton density and ion pressure show almost no changes with radial distance. Within the 70–100 R_J range, the proton density remains approximately 0.003 cm^{-3}, while the pressure of protons and heavy ions remains ∼0.005 and ∼0.03 nPa, respectively. This feature could be attributed to various factors, such as a termination of

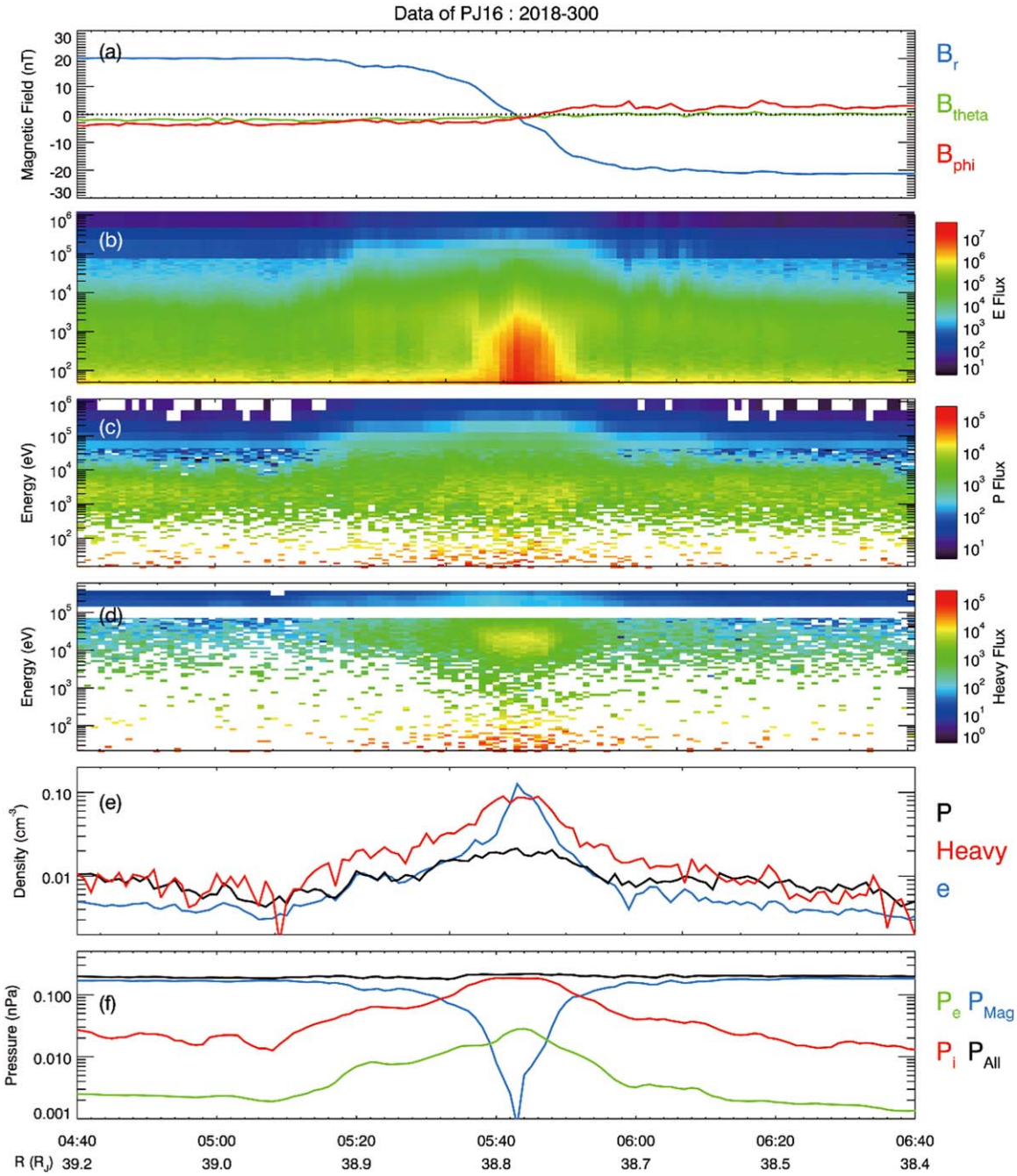

Figure 3. Results of a current-sheet crossing observed by the Juno spacecraft. Panel (a) represents the three-component magnetic field in the JSO spherical coordinate. Panels (b)-(d) represent the energy spectra of electrons, protons, and heavy ions, respectively. Panel (e) shows the calculated ion density, including electrons(blue), protons (black), and heavy ions (red). Panel (f) indicates the calculated pressure, including ions (red), electrons (green), magnetic (blue), and total (black) pressure.

plasma outflow near the magnetopause or a potential contribution of protons from the external solar wind.

3.3. Latitudinal Distribution of Plasma Properties

In the Jovian plasma sheet, plasma properties also exhibit latitudinal variations. We use the ratio between the local magnetic pressure and the lobe magnetic pressure $p = \frac{P_{Br}}{\overline{P}_{Br\_\mathrm{Lobe}}} = \frac{B_r^2}{\overline{B}_{r\_\mathrm{Lobe}}^{-2}}$ to describe the relative position to the plasma sheet, where P_{Br} indicates the magnetic pressure contributed by the B_r component and $\overline{P}_{Br\_\mathrm{Lobe}}$ indicates the average magnetic pressure in the corresponding lobe region. The factor $p = 0$ indicates that the spacecraft is at the center of the plasma sheet, while $p = 1$ indicates that the spacecraft is near the lobe. Figure 6 illustrates the variation of the median and quartiles of the densities of protons, heavy ions, and electrons with the factor p. As the distance to the current-sheet center increases, the ion density decreases, with a particularly significant decrease in the heavy ions. In the central region of the plasma sheet ($p < 0.5$), the proton density is lower than that of heavy ions, while in the outer regions of the plasma sheet ($p > 0.5$), the proton density is similar to or even higher than that of heavy ions. Additionally, the plasma density between 60 and 80 R_J is higher than that in the 80–100 R_J range at the center of the plasma sheet, while the plasma density

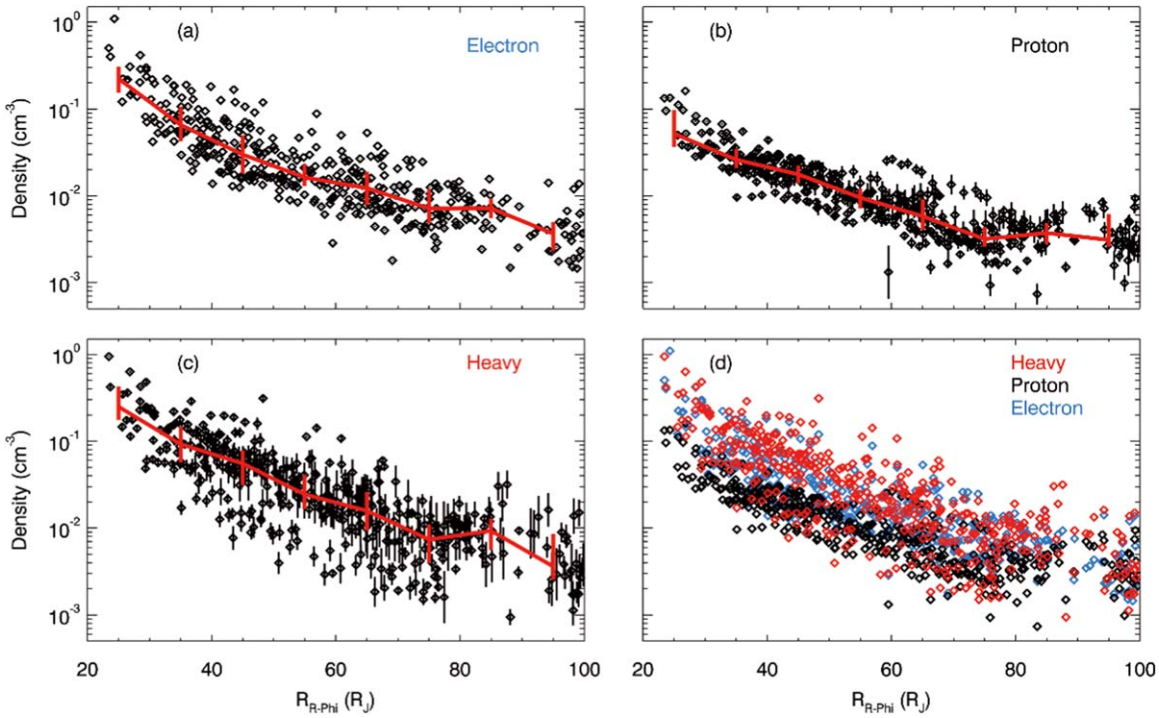

Figure 4. Radial distributions of plasma density in the current-sheet center. Panels (a)–(c) represent the radial distributions of the plasma density of electrons, protons, and heavy ions, respectively. Figure 3(d) compares these distributions. The red lines in panels (a)–(c) represent the median and quartiles in 10 R_J ranges. The size of the symbols has no specific meaning.

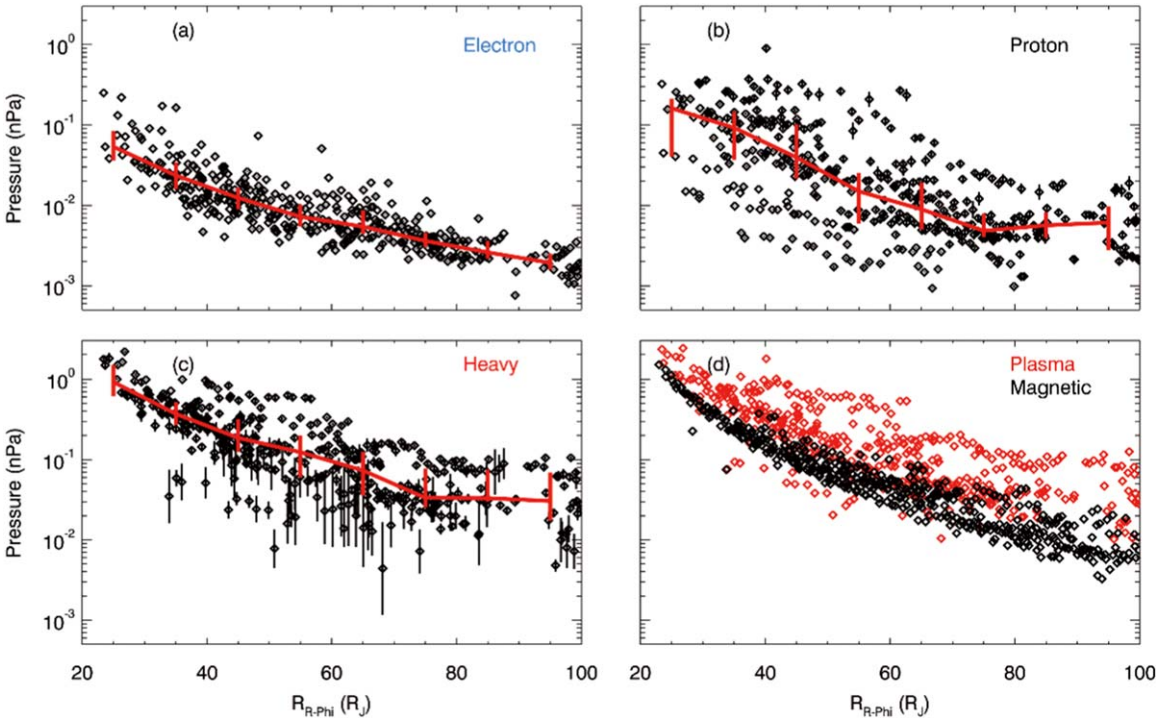

Figure 5. Radial distributions of plasma pressure at the current-sheet center. Panels (a)–(c) represent the pressure distribution of electrons, protons, and heavy ions with radial distance, respectively. Panel (d) shows the total plasma pressure (including electrons, protons, and heavy ions; red) and the distribution of magnetic pressure (black) in the 468 lobe regions obtained in Section 2.3. The red lines in panels (a)–(c) represent the median and quartiles in 10 R_J ranges. The size of the symbols has no specific meaning.

around 80–100 R_J in the lobe region is comparable to that in the 60–80 R_J range. This suggests that the plasma sheet may become thicker, and the distribution of ions is more dispersed at larger radial distances.

Figure 7 presents the latitudinal pressure distribution of protons, heavy ions, and electrons. In the center of the plasma sheet, the pressure of heavy ions is significantly larger than that of protons and electrons, consistent with the results shown in

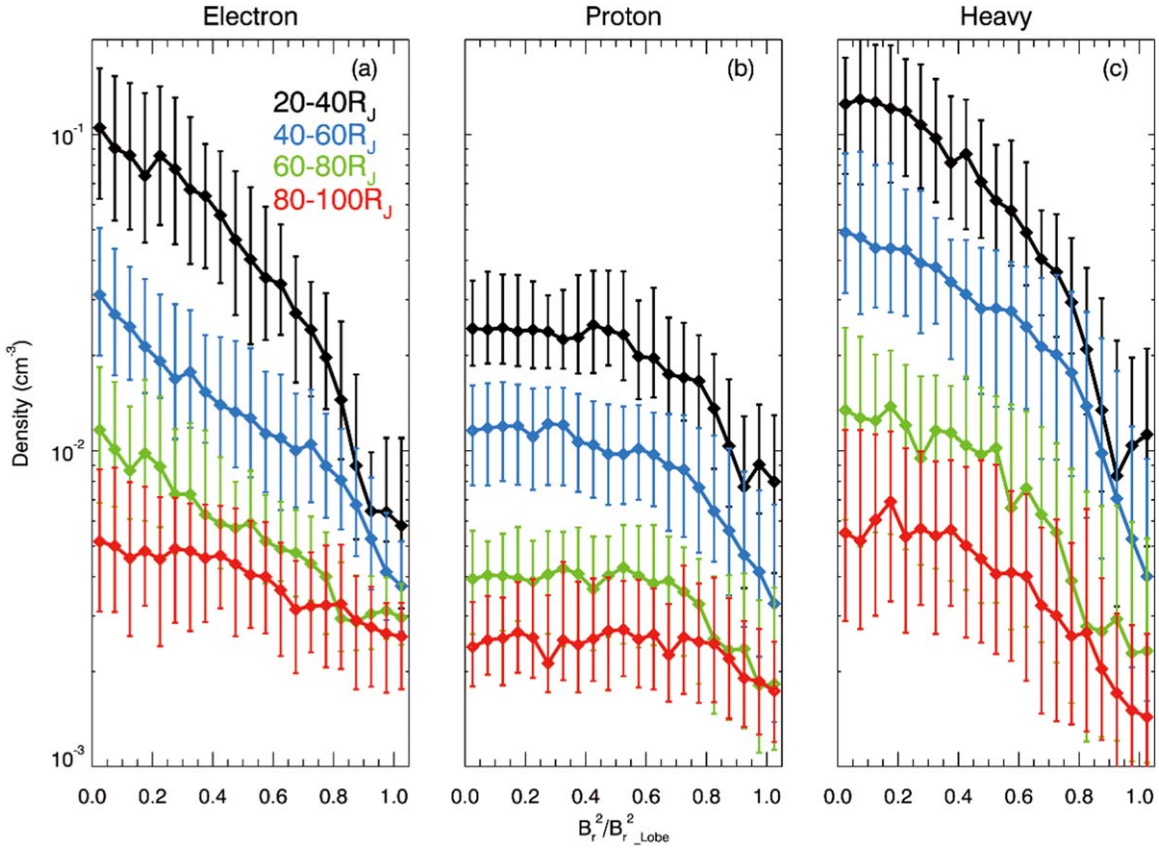

Figure 6. Distribution of plasma density in the latitudinal direction as a function of the factor $p = B_r^2/B_{r\_\mathrm{lobe}}^2$ described in Section 3.3. Panels (a)–(c) show the density median and quartiles of electrons, protons, and heavy ions from the center to the edge of the current sheet. Different colors indicate different radial distances.

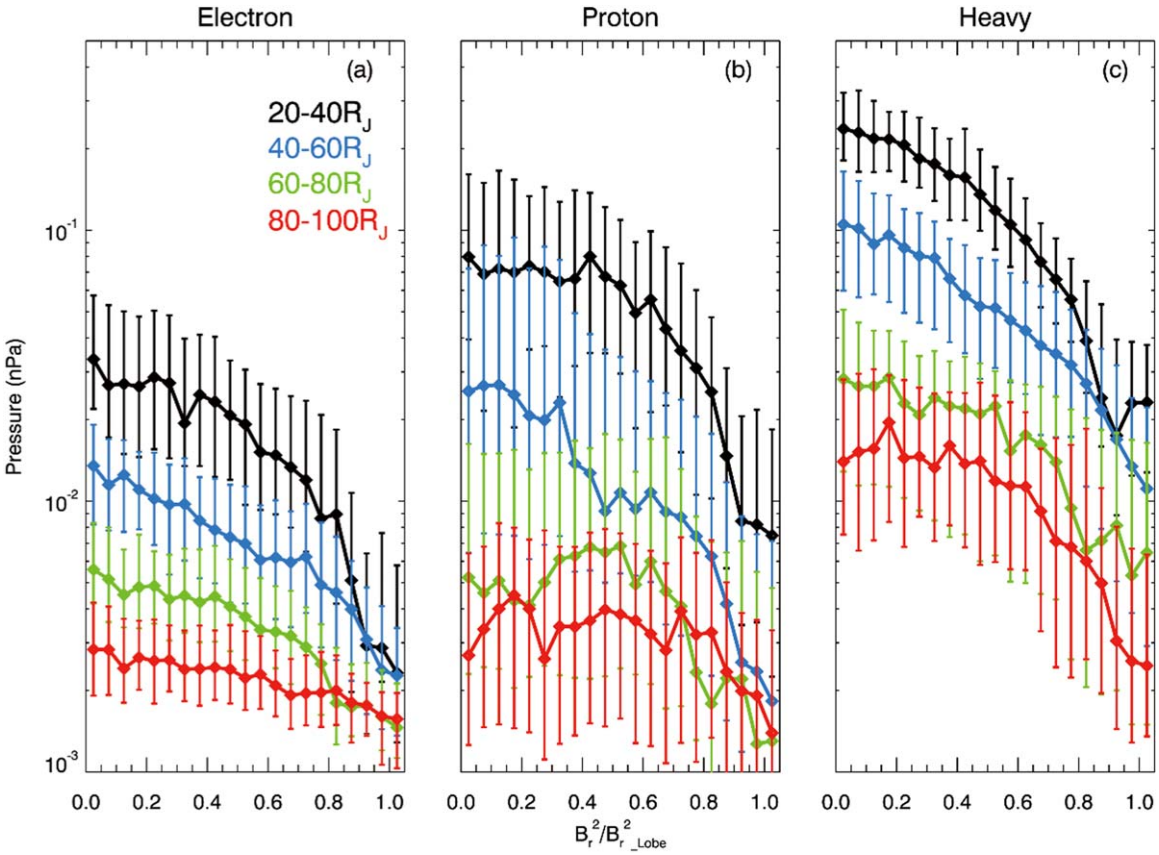

Figure 7. Similar to Figure 6 but represents the pressure distribution of the three plasma components from the center to the edge of the current sheet.

Figure 5. The pressure of heavy ions decreases as it moves away from the plasma sheet center and becomes near an order of magnitude smaller at the edge of the plasma sheet. Electron and proton pressure at the edge of the plasma sheet is about 1 order of magnitude lower than at the center around 20–40 R_J. However, as radial distance increases, the difference in electron and proton pressure between the center and edge of the plasma sheet gradually decreases. The proton pressure even demonstrates local peaks around $p = 0.5$ when the radial distance is larger than 60 R_j. Around 80–100 R_J, the electron and proton pressure at the edge of the plasma sheet is much closer to that at the center. It should be noted that near 80–100 R_J , there are fewer data points, which may cause larger uncertainty of plasma pressure at this region.

As shown in Figures 6 and 7, although the uncertainty of electrons is much lower than that of ions, the difference between their upper and lower quartiles roughly shows the same order of magnitude as that of ions, indicating that the distribution width of plasma parameters for different components is consistent. In the center of the plasma sheet at 60–80 R_J and 80–100 R_J, there is little difference in the ion pressure, consistent with the results of Section 3.2. However, at the edge of the plasma sheet, ion density and pressure at 80–100 R_J are close to—or even slightly larger than—those at 60–80 R_J, possibly due to the compression of the plasma sheet plasma during its outward transport toward the Jovian magnetopause and to the possible intrusion of solar wind plasma.

4. Discussion

In our study, we aimed to provide a statistical description of plasma properties within the Jovian plasma sheet. By combining magnetic field data from the Juno MAG instrument and particle observations from JADE and JEDI, we statistically analyzed the plasma density and pressure of different plasma components within the range of 20–100 R_J. Our findings shed light on the variations in plasma properties, magnetic pressure balance, and latitudinal distribution within the plasma sheet. The electron density in the center of the plasma sheet is observed to decrease from approximately 0.5 cm^{-3} near 20 R_J to 0.003 cm^{-3} near 100 R_J. Similarly, the plasma pressure decreases from around 2 nPa at 20 R_J to 0.03 nPa at 100 R_J. The dominant contribution to the pressure at the plasma sheet center comes from heavy ions, which were roughly in balance with the magnetic pressure in the lobe region. At radial distances larger than 70 R_J, proton density and ion pressure show minimal variation with radial distance. Furthermore, the density and pressure of heavy ions rapidly decrease by nearly an order of magnitude from the center of the plasma sheet to the edge of the plasma sheet, and variations in the plasma properties of protons between the center and edge of the plasma sheet exhibit a radial distance dependence. At radial distances closer to Jupiter (20–40 R_J), differences in density and pressure between the center and edge are significant. However, at larger distances (60–100 R_J), these differences decrease, suggesting a more uniform distribution of plasma properties within the plasma sheet.

Figures C1–C2 compare our results with previous models and observational studies. In Figure C1, we compared our plasma densities with the model results given by Bagenal & Delamere (2011) and Dougherty et al. (2017). For $R < 50$ R_J, our electron density is consistent with Bagenal & Delamere (2011) but lower than that of Dougherty et al. (2017). However, for $R > 50$ R_J, our results are slightly lower than those of Bagenal & Delamere (2011). The proton density profile is similar to that obtained by Dougherty et al. (2017), while the density profile of heavy ions derived by Dougherty et al. (2017) is slightly larger compared with our statistical result, especially for $R > 50$ R_J.

Figure C2 compares the plasma pressures obtained in our study and those from Mauk et al. (2004). We also plot pressure product derived from the density obtained by Dougherty et al. (2017) and temperature obtained by Kim et al. (2020b; $T_{proton} \sim 3$ keV and $T_{heavy} \sim 10$ keV) for further comparison. The proton pressure in our study is slightly higher than those in the previous results, which are still within our distribution range. The heavy ion pressure obtained in our study is almost identical to those previous results.

While previous studies of Jovian plasma sheet beyond 50 R_J have been limited, our study uses in situ observations by Juno and extends the observations of plasma properties from 20 R_J to 100 R_J. Consistent with Liu et al. (2021), who observed an increased thickness of the plasma sheet beyond 70 R_J and no significant radial variation in high-energy ion fluxes, we find minimal changes in ion pressure and proton density at radial distances beyond 70 R_J. These observations suggest that radial transport on the Jovian magnetosphere dawnside may be inhibited by the proximity of the magnetopause and suggest a possible influence of solar wind plasma inflow.

The latitudinal distribution of plasma properties also exhibits significant variations within the Jovian plasma sheet. Heavy ions have a higher number density at the center of the current sheet, while protons are more dispersed in the latitudinal direction, consistent with previous Juno and Voyager studies (e.g., Bodisch et al. 2017; Dougherty et al. 2017; Huscher et al. 2021). Moreover, the differences between the center and edge of the plasma sheet depend on radial distance. The pressure ratio between the center and edge remains nearly an order of magnitude for heavy ions, while the proton pressure ratio decreases significantly with the increase of radial distance. These variations may be the combined effect of the field-aligned polarization electric field and the different centrifugal forces acting on the different plasma components, as studied by Maurice et al. (1997).

Due to multiple factors like the different condition and MLT locations at Juno's different Perijoves, the plasma pressure and number density vary at the same radial distance. This limitation makes it challenging to calculate the current density based on the plasma pressure gradient. In addition, it is important to note that the low ion count rates from the JADE instrument, due to the slow velocities of ions, introduce uncertainties in ion measurements, particularly for ions with energy below ~1 keV (see error bars in Figures 2 and B1–B4). We used the average value over an extended period (~20 minutes) to improve the signal-to-noise ratio of the calculated plasma properties through error propagation. The uncertainty is generally smaller than the differences between various cases with heavy ions having relatively larger uncertainties, especially beyond ~ 70 R_J (see error bars in Figures 4 and 5).

Overall, our results provide valuable insights into the plasma properties of the Jovian plasma sheet, utilizing comprehensive data from the Juno mission. They contribute to a wider view of the Jovian plasma characteristics, including their radial and latitudinal distribution, and the overall pressure balance of the Jovian plasma sheet.

5. Conclusions

In this study, we conducted a comprehensive analysis of the plasma properties of the Jovian plasma sheet using data obtained from the Juno spacecraft during its first 31 orbits. By examining 419 observed plasma sheet crossings at radial distances ranging from $20\,R_{\rm J}$ to $100\,R_{\rm J}$, we reached the following conclusions:

1. The electron number density within the plasma sheet decreases as the radial distance $R_{\rm R\text{-}Phi}$ increases from $20\,R_{\rm J}$ to $100\,R_{\rm J}$, with values dropping from approximately 0.5 to $0.003\,{\rm cm}^{-3}$. Additionally, heavy ion densities are found to be larger at the center of the plasma sheet, and proton densities are more dispersed.
2. The plasma pressure within the plasma sheet is predominantly contributed by heavy ions. It decreases from around 2 nPa at $20\,R_{\rm J}$ to 0.03 nPa at $100\,R_{\rm J}$. The plasma pressure within the plasma sheet center is basically balanced by the magnetic pressure in the lobe region.
3. The density and pressure of heavy ions consistently drop about an order of magnitude from the center to the edge of the plasma sheet. However, for protons, this ratio decreases with increasing radial distance.
4. Beyond $70\,R_{\rm J}$, variations observed at the center of the plasma sheet in proton number density and ion pressure are very limited. This phenomenon may be attributed to the inhibition of plasma outflows near the magnetopause on the Jovian dawnside, to a possible inflow of plasma from the solar wind, and/or to upward transport of plasma from the Jovian ionosphere.

Acknowledgments

The study was supported by NSFC research grant 42274200. The authors acknowledge the use of data from NASA Planetary Plasma Interactions Node, including the MAG data (Connerney; 2017; https://pds-ppi.igpp.ucla.edu/collection/JNO-J-3-FGM-CAL-V1.0), the JADE data (Allegrini et al. 2022; https://pds-ppi.igpp.ucla.edu/data/JNO-J_SW-JAD-5-CALIBRATED-V1.0/DATA/), and the JEDI data (Mauk 2022; https://pds-ppi.igpp.ucla.edu/data/JNO-J-JED-3-CDR-V1.0/DATA/).

Appendix A
Energy/q-TOF Relation of Ions

In this appendix, we present the measurement of E/q-TOF relation measured by the JADE-TOF on 2018 October 27 in Figure A1. Different ion components measured by the instrument and the m/q range in this study are also shown in the figure.

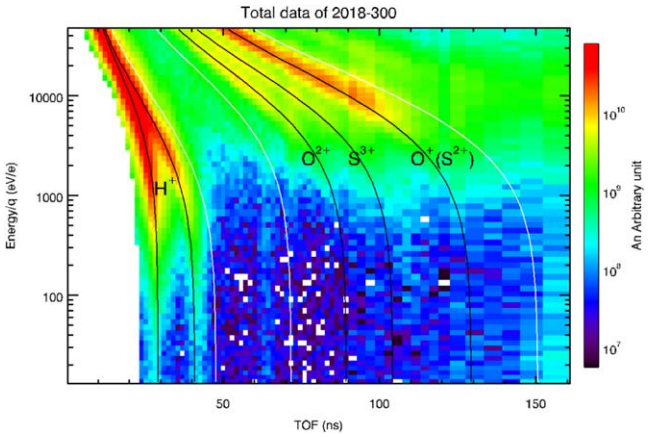

Figure A1. Energy/q-TOF relation measured by the JADE-TOF instrument. The black lines indicate the E/q-TOF curves of different ion components. Due to the carbon foil effect, protons have two E/q-TOF curves (see Kim et al. 2020a for details). The white lines indicate the E/q-TOF boundaries of protons and heavy ions in this study.

Appendix B
Energy Spectra beyond 60 R_J

In this appendix, we present distributions of flux of electrons, protons, and heavy ions during the 10 minutes before and after the current-sheet crossings at different radial distances of 66.8, 75.2, 86.1, and 96.3 R_J in Figures B1–B4, respectively.

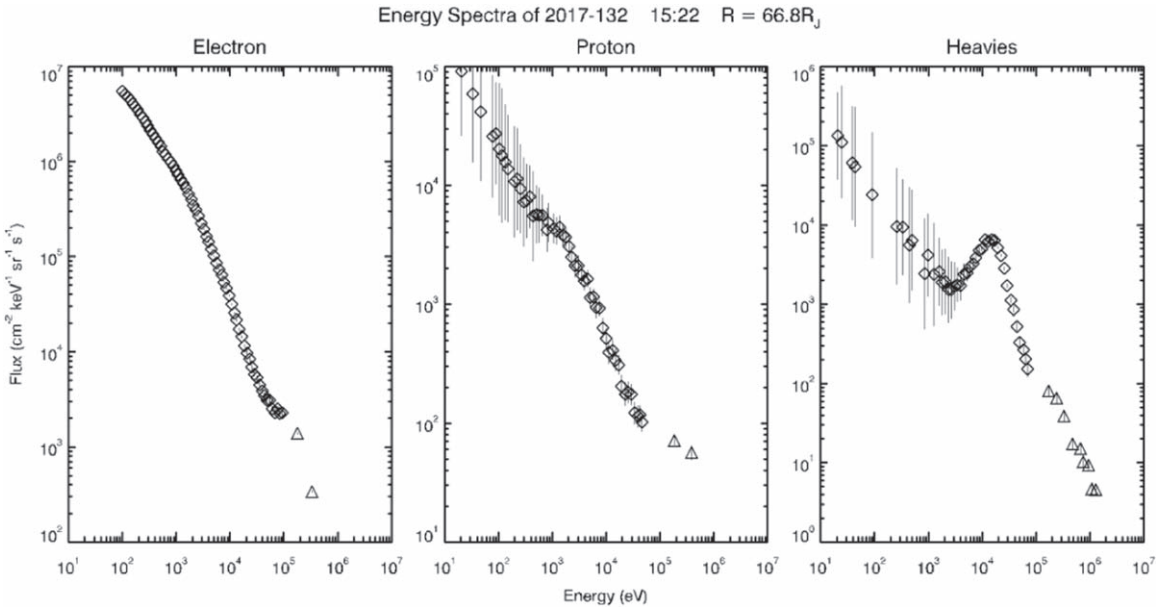

Figure B1. Energy spectra of (left) electrons, (middle) protons, and (right) heavy ions during the plasma sheet crossing at 15:22 on 2017 May 12 at 66.8 R_J from Jupiter. The diamonds represent data from the JADE instrument, while the triangles represent data from the JEDI suite. The size of the symbols has no specific meaning.

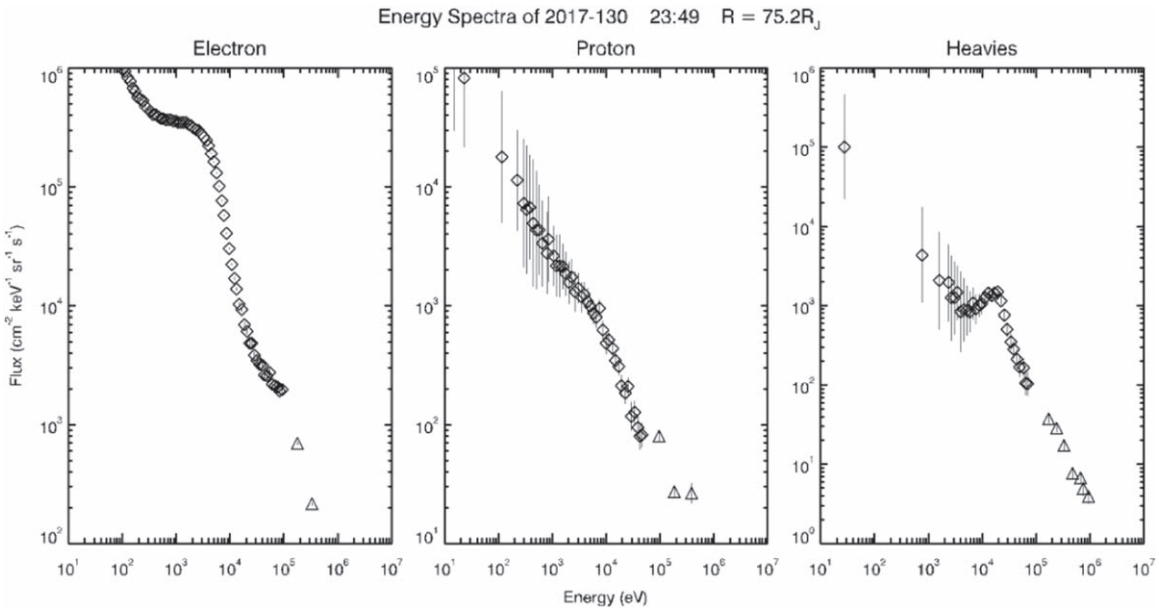

Figure B2. Like Figure A1 but for the plasma sheet crossing at 23:49 on 2017 May 10 at 75.2 R_J from Jupiter.

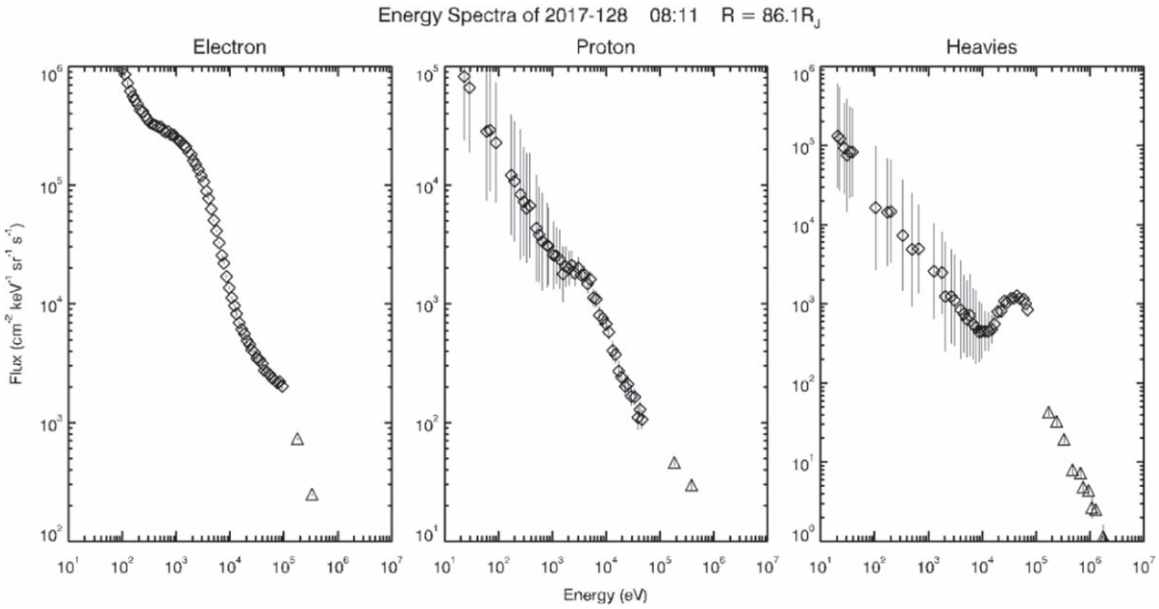

Figure B3. Like Figure A1 but for the plasma sheet crossing at 08:11 on 2017 May 8 at 86.1 R_J from Jupiter.

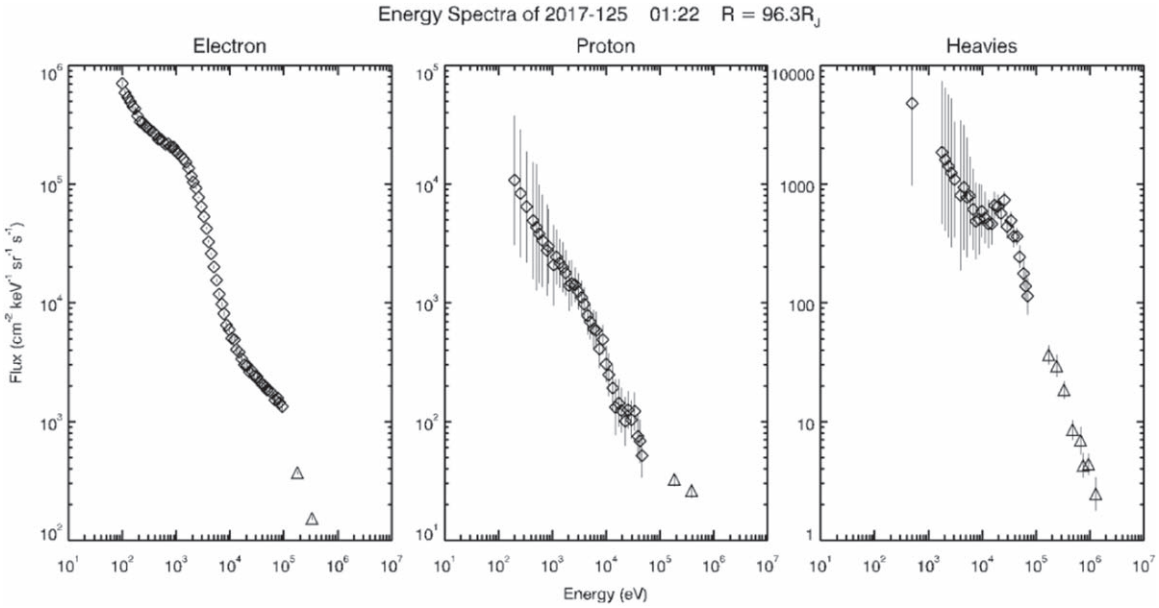

Figure B4. Like Figure A1 but for the plasma sheet crossing at 01:22 on 2017 May 5 at 96.3 R_J from Jupiter.

Appendix C
Comparisons with Previous Studies

In this appendix, we present comparisons with density provided by Bagenal & Delamere (2011) and Dougherty et al. (2017) in Figure C1 and pressure provided by Mauk et al. (2004) in Figure C2. For further comparison, the pressure product is derived from the density provided by Dougherty et al. (2017), and the temperature provided by Kim et al. (2020b; ∼3 keV for protons and ∼10 keV for heavy ions) as shown in Figure C2.

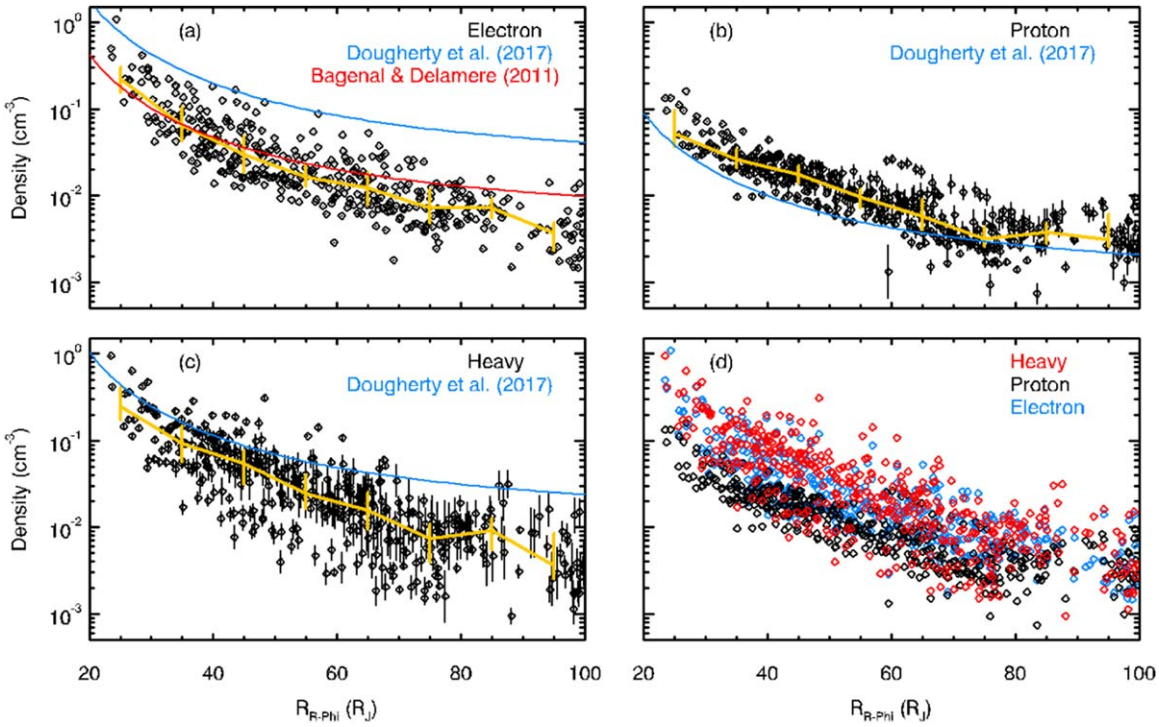

Figure C1. Density comparisons with previous studies. Black points in panels (a)–(c) represent the densities obtained in this study, while densities given by Dougherty et al. (2017) and Bagenal & Delamere (2011) are in blue and red, respectively.

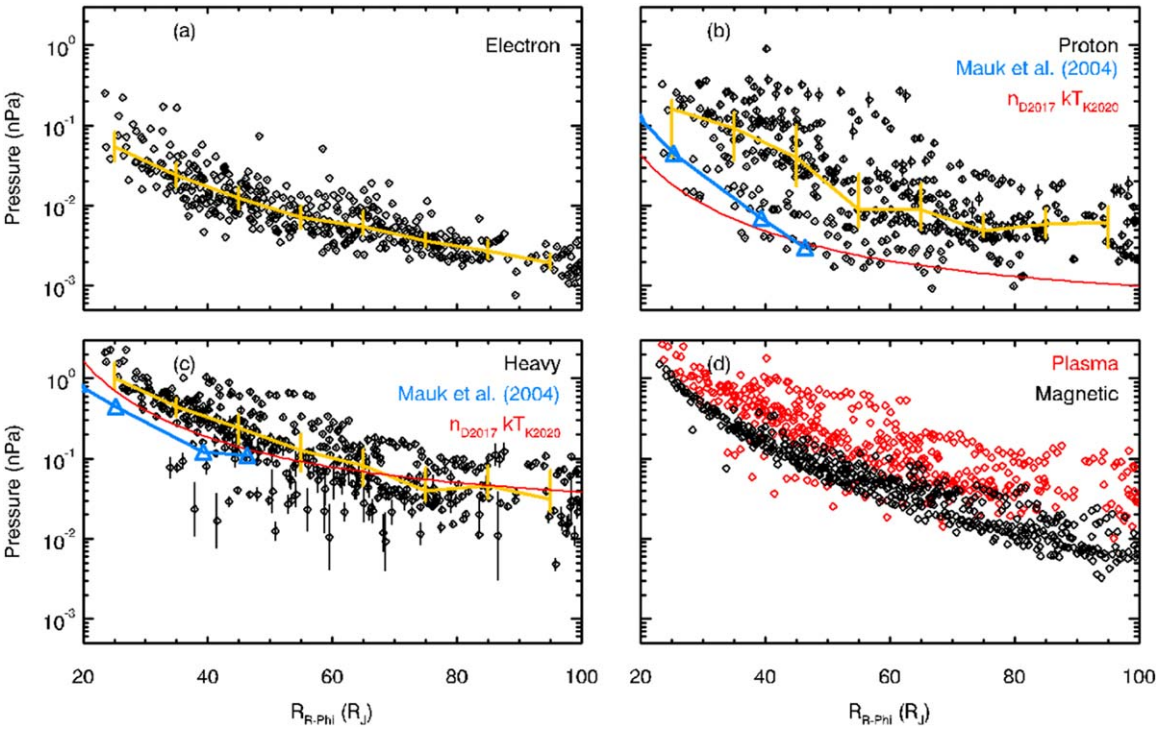

Figure C2. Pressure comparisons with previous studies. Black points in panels (a)–(c) represent the pressure obtained in this study, while pressure given by Mauk et al. (2004) and the product of density provided by Dougherty et al. (2017), and temperature from Kim et al. (2020b) are in blue and red, respectively.

ORCID iDs

Haobo Fu https://orcid.org/0000-0002-0857-8910
Chao Yue https://orcid.org/0000-0001-9720-5210

References

Allegrini, F., Gladstone, G. R., Hue, V., et al. 2020, GeoRL, 47, e2020GL089732
Allegrini, F., Kruth, W. S., Elliott, S. S., et al. 2021, JGRA, 126, e2021JA029426
Allegrini, F., Wilson, R. J., Ebert, R. W., et al. 2022, Juno JADE Derived Science Data, NASA Planetary Data System, doi: 10.17189/2775-4623
Bagenal, F. 1994, JGR, 99, 11043
Bagenal, F., Adriani, A., Allegrini, F., et al. 2017a, SSRv, 213, 219
Bagenal, F., & Delamere, P. A. 2011, JGRA, 116, A05209
Bagenal, F., & Dols, V. 2020, JGRA, 125, e2019JA027485
Bagenal, F., Dougherty, L. P., Bodisch, K. M., Richardson, J. D., & Belcher, J. M. 2017b, JGRA, 122, 8241
Bagenal, F., Wilson, R. J., Siler, S., Paterson, W. R., & Kurth, W. S. 2016, JGRE, 121, 871
Bandyopadhyay, R., Begley, L. J., Maruca, B. A., et al. 2022, GeoRL, 49, e2022GL098053
Bodisch, K. M., Dougherty, L. P., & Bagenal, F. 2017, JGRA, 122, 8277
Connerney, J. E. P. 2017, Juno J Fluxgate Magnetometer Calibrated Data V1.0. NASA Planetary Data System, doi: 10.17189/1519711
Connerney, J. E. P., Benn, M., Bjarno, J. B., et al. 2017, SSRv, 213, 39
Connerney, J. E. P., Kotsiaros, S., Oliverson, R. J., et al. 2018, GeoRL, 45, 2590
Connerney, J. E. P., Timmins, S., Herceg, M., & Joergensen, J. L. 2020, JGRA, 125, e2020JA028138
Cowley, S. W. H., & Bunce, E. J. 2001, P&SS, 49, 1067
Cowley, S. W. H., Bunce, E. J., & Nichols, J. D. 2003, JGRA, 108, 8002
Dougherty, L. P., Bodisch, K. M., & Bagenal, F. 2017, JGRA, 122, 8257
Hill, T. W. 1979, JGRA, 84, 6554
Huscher, E., Bagenal, F., Wilson, R. J., et al. 2021, JGRA, 126, e2021JA029446
Kim, T. K., Ebert, R. W., Valek, P. W., et al. 2020a, JGRA, 125, e2018JA026169
Kim, T. K., Ebert, R. W., Valek, P. W., et al. 2020b, JGRA, 125, e2019JA027696
Khurana, K., Vasyliūnas, V., Mauk, B., et al. 2004, Jupiter: The Planet, Satellites and Magnetosphere (Cambridge: Cambridge Univ. Press), 593
Krupp, N., Vasyliūnas, V., Woch, J., et al. 2004, The Dynamics of the Jovian Magnetosphere. Jupiter: The Planet, Satellites and Magnetosphere (Cambridge: Cambridge Univ. Press), 617
Liu, Z.-Y., Zong, Q.-G., Blanc, M., et al. 2021, JGRA, 126, e2021JA029710
Ma, Q., Li, W., Zhang, X.-J., et al. 2021, GeoRL, 48, e2021GL095833
Mauk, B. H. 2022, JEDI Calibrated (CDR) Data JNO J JED 3 CDR V1.0, NASA Planetary Data System, doi: 10.17189/1519713
Mauk, B. H., Allegrini, F., Bagenal, F., et al. 2022, JGRA, 127, e2022JA030293
Mauk, B. H., Haggerty, D. K., Jaskulek, S. E., et al. 2017, SSRv, 213, 289
Mauk, B. H., Mitchell, D. G., McEntire, R. W., et al. 2004, JGRA, 109, A09S12
Mauk, B. H., Szalay, J. R., Allegrini, F., et al. 2023, JGRA, 128, e2022JA031237
Maurice, S., Blanc, M., Prangé, R., & Sittler, E. C. 1997, P&SS, 45, 1449
McComas, D. J., Alexander, N., Allegrini, F., et al. 2017, SSRv, 213, 547
Nichols, J. D., Achilleos, N., & Cowley, S. W. H. 2015, JGRA, 120, 10
Ranquist, D. A., Bagenal, F., Wilson, R. J., et al. 2019, JGRA, 124, 9106
Szalay, J. R., Clark, G., Livadiotis, G., et al. 2022, GeoRL, 49, e2022GL098741
Thomas, N., Bagenal, F., Hill, T. W., & Wilson, J. K. 2004, The Io Neutral Clouds and Plasma Torus (Cambridge: Cambridge Univ. Press)
Vasyliunas, V. M. 1983, in Physics of the Jovian Magnetosphere, ed. A. J. Dessler (Cambridge: Cambridge Univ. Press), 395
Wang, J.-z., Bagenal, F., Wilson, R. J., et al. 2024, JGRA, 129, e2023JA032218
Wang, Y., Blanc, M., Louis, C., et al. 2021, JGRA, 126, e2021JA029469